www.czasopisma.pan.pl PAN POLSKA AKADEMIA NAUK www.journals.pan.pl

A R C H I V E S O F M E T A L L U R G Y A N D M A T E R I A L S

Volume 56 2011 Issue 2

DOI: 10.2478/v10172-011-0028-6

H. PAUL[*, **], T. BAUDIN[***], F. BRISSET[***]

THE EFFECT OF THE STRAIN PATH AND THE SECOND PHASE PARTICLES ON THE MICROSTRUCTURE AND THE TEXTURE EVOLUTION OF THE AA3104 ALLOY PROCESSED BY ECAP

WPŁYW SCHEMATU ODKSZTAŁCENIA ORAZ CZĄSTEK DRUGIEJ FAZY NA ROZWÓJ MIKROSTRUKTURY I TEKSTURY STOPU AA3104 PRZETWARZANEGO METODĄ WYCISKANIA W KANALE RÓWNOKĄTOWYM

The effect of the strain path on the microstructure and the texture evolution of the severely deformed AA3104 aluminium alloy was investigated by a transmission electron microscopy (TEM) and a high resolution scanning electron microscopy (SEMFEG) equipped with the electron backscattered diffraction facility. A commercial purity material was deformed at room temperature *via* equal channel angular pressing up to 10 passes, following the routes A, B_C, and C.

A good quality billet after 10 passes was obtained only in the case of route C. In the case of route A and B_C, macro-cracking appeared after 5 and 3 passes, respectively. Although the different routes led to differences in the microstructure of the billets, the global texture evolution turned out to follow nearly the same 'course'. The TEM observations and the SEMFEG local orientation measurements allowed to identify the misoriented planar dislocation arrangements in all the samples. Their instability within some narrow areas led to the kink-type bands, which were precursors of the shear bands. The influence of the second phase particles on the deformation microstructure and the local texture depended on the particle size. Irrespective of the applied deformation routes, the large (>5 μm), not deformable second phase particles influenced the strengthening of the matrix by forming local distortions in their vicinity, whereas the fine dispersoids (~50 nm) had a visibly unclear effect on the dislocation structures formed in the examined strain range.

Keywords: ECAP, Microstructure, Texture, Shear band, Aluminium alloy

W pracy analizowano wpływ zmiany drogi odkształcenia na ewolucję mikrostruktury i tekstury silnie odkształcanych próbek stopu aluminium - AA3104, wykorzystując techniki transmisyjnej (TEM) i skaningowej (SEMFEG) mikroskopii elektronowej. Materiał o czystości technicznej odkształcano w temperaturze otoczenia, w matrycy równo kątowej (ECAP) do 10-ciu przepustów, wg drogi A, B_C oraz C.

Wyniki prowadzonych analiz pokazują, że jedynie w przypadku drogi C uzyskano po 10-ciu przepustach dobry jakościowo 'wstępniak'. W przypadku drogi A i B_C po 5 i 3 przepustach, odpowiednio, pojawiały się obserwowane makroskopowo pęknięcia. Pomimo, że zróżnicowane drogi odkształcenia prowadzą do silnego zróżnicowania w obrazie mikrostruktury, ewolucja tekstury globalnej jest podobna. Obserwacje mikrostrukturalne prowadzone w skali TEM oraz pomiary orientacji lokalnych z wykorzystaniem techniki SEMFEG dokumentują formowanie się płaskich układów dyslokacyjnych, niezależnie od zastosowanego schematu odkształcenia. Dodatkowo obserwowana wewnątrz wąskich obszarów niestabilność tych struktur prowadzi do pojawienia się pasm ugięcia które są prekursorami pasm ścinania. Wpływ cząstek drugiej fazy na ewolucję struktury odkształcenia oraz zmiany w 'lokalnym obrazie tekstury' w pobliżu cząstek, silnie uzależnione są od rozmiaru cząstek. Jednakże, niezależnie od zastosowanego schematu odkształcenia, duże (>5 μm) nieodkształcalne cząstki silnie determinują umocnienie osnowy w ich bezpośrednim sąsiedztwie, podczas gdy wpływ drobnych wydzieleń dyspersyjnych (~50 nm) nie jest jasno zdefiniowany.

1. Introduction

In the recent years, severe plastic deformation (SPD) has very often been used for the improvement of the strength properties of aluminium alloys by means of converting the conventional coarse-grained metals into ultra-fine grained metals [1]. An equal channel angular pressing (ECAP) is one of the variants of the SPD methods. It involves the use of a die that contains two

[*] INSTITUTE OF METALLURGY AND MATERIALS SCIENCE, POLISH ACADEMY OF SCIENCES, 25 REYMONTA ST., 30-059 KRAKÓW, POLAND

[**] FACULTY OF MECHANICS, OPOLE UNIVERSITY OF TECHNOLOGY, 5 MIKOŁAJCZYKA ST., 45-271 OPOLE, POLAND

[***] UNIVERSITÉ PARIS-SUD, ICMMO, CNRS UMR 8182, LABORATOIRE DE PHYSICO-CHIMIE DE L'ETAT SOLIDE, ORSAY, F-91405, FRANCE

intersecting channels of equal cross-section and, among other SPD techniques, has the advantage of producing relatively large samples. This provides the possibility to manufacture the required material at the industrial level and also has the potential for commercialization.

It was frequently reported in the past that four processing routes could be used in ECAP. Their application leads to different structures and a different degree of the grain refinement [1-9]. In route A, the specimen is pressed without rotation. In route B_A, the specimen is rotated (around the extrusion direction (ED)) by 90° in alternate directions between the consecutive passes, whereas in routes B_C and C, the specimens are rotated by 90° and 180° counterclockwise between each pass, respectively. In the case of the material processed through route A, the flat dislocation arrangements have a tendency to align along the ED-TD plane, where TD is the transverse direction. Route B_C, in fact, describes the re-orientation of the dislocation microstructures around ED, superimposed upon rotation around TD, due to the shear plane inclination effect. This should therefore lead to the desired nearly equiaxed structure [2, 10]. In the case of route C, the shear plane and the shear reversal effects combine.

Earlier studies have led to contradictory conclusions concerning the final properties as a 'function' of the pass number. On the one hand, there is some evidence for the absence of strain hardening as the number of passes increases, e.g. [10-12]. In that case, the samples can be processed up to extremely large strains. On the other hand, due to the strong increase of the dislocation density, the decomposition of the billets in the macro-scale is often observed [8-10, 13]. This limits further room temperature processing.

The properties of the deformed samples depend not only on the pass number and the applied deformation route but also on the microstructural variables associated with the initial material [14-18]. In particular, the combined effects of the small dispersoids and/or the large particles on the microstructure development are in the centre of interest. In the two phase alloys containing the second phase particles (SPP), the diameter, shape and the uniform or non-uniform distribution of the particles are crucial for the dislocation structure development and determines the processing ability of the material [11, 19-23].

One of the most popular (and industrially important) aluminium alloys which contains many non-deformable second phase particles is the AA3104 alloy. Recently, Yao et al [22] and Liu et al [23] have investigated the microstructure and the texture evolution during the cold rolling of the AA3104 alloy. Upon deformation of the matrix containing large non-deformable particles, the deformation incompatibilities occur at the matrix/particle interfaces and lead to the formation of deformation zones around the particles. In the ECAP-processed samples, the deformations in the volumes of the matrix close to the coarse particles are increased by the shear plane effect. The presence of fine non shareable dispersoids has been found to reduce the rate of the high angle boundary generation, and hence, it retards the formation of a submicron grain structure to higher strains, as shown, e.g. by Apps et al [21] in the model Al-0.2%Sc alloy.

In the present study, the main effort has been directed towards elucidating the influence of the combined effect of the deformation path and the second phase particles on the microstructure and texture development during the ECAP deformation of the AA3104 aluminium alloy. This has been done by the application of microstructure characterization techniques in a transmission electron microscope (TEM) and local orientation measurements in a high resolution scanning electron microscope (SEMFEG) equipped with the electron backscattered diffraction (EBSD) facility. This combination of experimental techniques allows for a detailed characterization of the dislocation structure and the distribution of the orientations over relatively large areas. A particular attention was paid to the formation of instabilities within the dislocation structure. The samples were deformed up to 10 passes through three different routes, i.e. A, B_C and C, and then analyzed on the basis of two sections, i.e. one perpendicular to ED and the other – to TD.

2. Experimental

The material used in the investigations was the commercial AA3104 aluminium alloy. The as-cast ingot was homogenized and then hot rolled on an industrial reversing mill to a 10 mm thick sheet. Samples with dimension of 10×10 mm^2 (cross section) and length of 70 mm (for ECAP) were machined from the sheet, and then annealed at 425°C for 1.5h and then slowly cooled. A grain of the size of 40-60 μm was revealed before processing. The initially prepared material was deformed *via* ECAP, through route A, B_C, and C, at room temperature, with the constant frame velocity of 0.5 mm/s, up to 10 passes (logarithmic strains of ~11). A square cross section ECAP die of 10×10 mm^2 was used, with the die angle of 90° and the outer corner radius of 5 mm, giving the nominal (von Mises) effective strain of ε_M = 1.115 [2]. The billet and tooling were well lubricated with MoS_2-containing grease. After each pass, the die was opened and the sample was removed from the die, re-polished and subjected to the next pass. The sample co-ordinate system is shown in Fig. 1.

The deformed samples were sectioned in two orientations through their centre, i.e. parallel to the ND-ED and ND-TD planes, where ND is the normal direction. For detailed TEM investigations, the samples were cut into slices and subsequently reduced in thickness from about 200 μm to about 60-80 μm by grinding with SiC papers, followed by twin jet electropolishing in a solution composed in one part of HNO_3 and two parts of CH_3OH, at -35°C, with the use of the voltage of 20.5 V. The chemical compositions of the matrix and the second phase particles were examined in an FEI Tecnai G^2 transmission electron microscope (TEM) equipped with a Gatan imaging filter and an EDAX spectrometer. An analytical double-tilt holder was used for the identification of the second phase particles. The microtexture evolution in the nanoscale was analyzed through local orientation measurements in TEM with the use of an in-house Kikuchi line based system, e.g. [9].

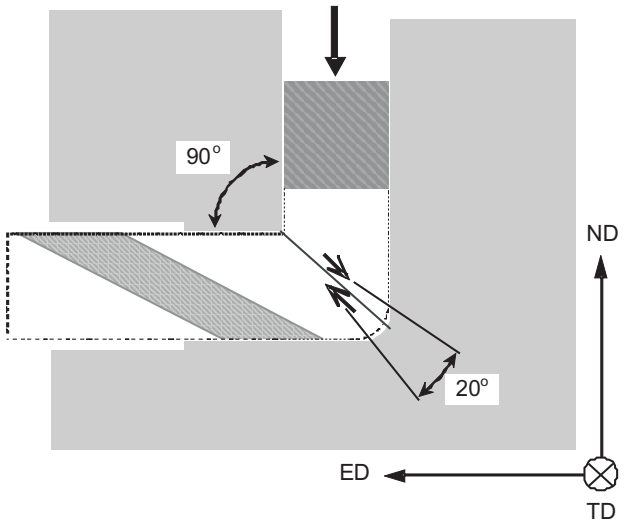

Fig. 1. Sample (die) geometry and external coordinate system during ECAP

The EBSD orientation maps were acquired with the use of FEG-SEM Zeiss Supra 55VP equipped with the EBSD pattern collection system, with the spatial resolution of ~50 nm and the angular resolution of ~1°. In that case, the pattern acquisition and the solution were carried out with the TSL OIM 5 software. The orientation maps were carried out in the automatic beam scanning mode using the step of 100 nm. The surfaces of the specimens taken from the section perpendicular to ED were mechanically ground with SiC paper, followed by paste containing diamond particles of 3 μm. The TEM thin foils were prepared by a twin-jet technique using TenuPol-5 in a standard Struers A2 solution (20V/5°C).

The SEM-FEG/EBSD local orientation measurements were compared with the global textures determined by the X-ray diffraction, by means of the Philips X'Pert system, equipped with the ATC3 texture goniometer. The samples for the texture measurement were cut from the middle portion of the extruded billets, where the steady-state deformation could be expected. The filtered X-ray radiation CoKα (λ=0.179026nm) was used. The set of incomplete pole figures of the selected {*hkl*} – planes was registered for the examined sample area (ca. 2.0 mm^2). The backreflection technique was used and the figures were measured in the range of α=0–75° and β=0–360° by the so-called Equal Solid Angle measurement grid, with 642 points at the regular pole figure window $\Delta\alpha/\Delta\beta$ = 1 [24]. The scintillation counter in the pseudo-position sensitive detection (*pPSD*) mode was applied in the measurements [25]. In order to estimate the level of strengthening, the measurements of the Vickers microhardness (by applying the load of 25 g for 10 s) in the plane perpendicular to ED were performed.

The deformation behaviour was studied using the plane strain compression (PSC) testing, on the specimens of the dimensions of 7mm (|| TD), 8 mm (|| ED) and 10 mm (|| ND). The samples were cut from the centre of each billet, polished, lubricated with Teflon^{TM} and then deformed at room temperature with the initial strain rate of $\sim 10^{-2}s^{-1}$ with the use of the INSTRON 3382 testing machine. The direction of the compression in the PSC test was parallel to the normal axis of the billet. Additionally, the coincidence between the other two directions in ECAP and PSC was conserved, i.e. ED_{ECAP}|| ED_{PSC} and TD_{ECAP}|| TD_{PSC}.

3. Results

3.1. Mechanical behaviour

It was found that the different routes led to differences in the quality, microstructure and mechanical behaviour of the billets. In the case of route A and B_C, the macro-cracking appeared after 5 and 3 passes, respectively. In the successive passes, the cracks propagate along the whole sample, as visible in Fig. 2, for the sample deformed along route A. In each case, the cracks start to propagate from the free end of the sample. The good quality of the billets after 10 passes was obtained only in the case of route C.

The experimentally measured values of microhardness and yield stress (samples tested in PSC) are presented in Fig. 3 as a 'function' of the ECAP pass number. As can be clearly seen, for the samples deformed through route C, the microhardness increases monotonically with a clear tendency to saturate at high strains (Fig. 3a). A slightly stronger increase of the microhardness in the first few passes is observed in the case of the samples deformed through routes A and B_C.

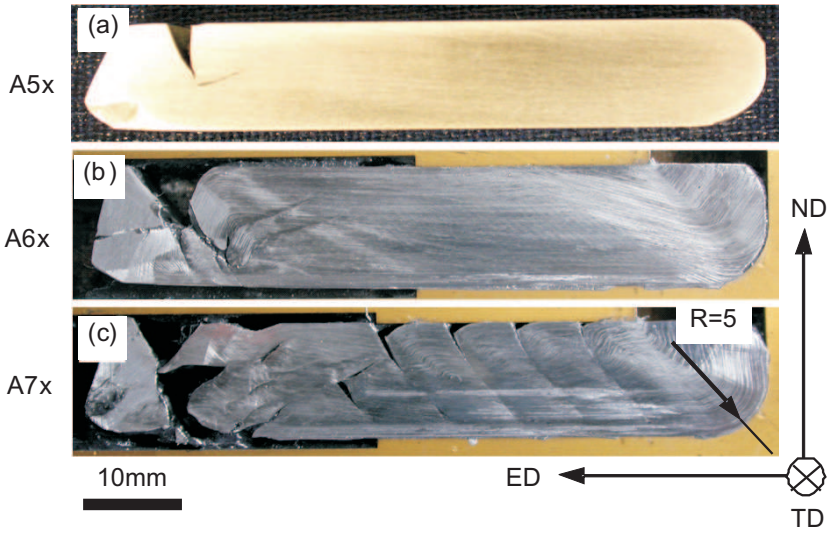

Fig. 2. Macro-cracks propagation in successive passes. Sample deformed through route A after: (a) 5, (b) 6 and (c) 7 passes. Optical microscopy

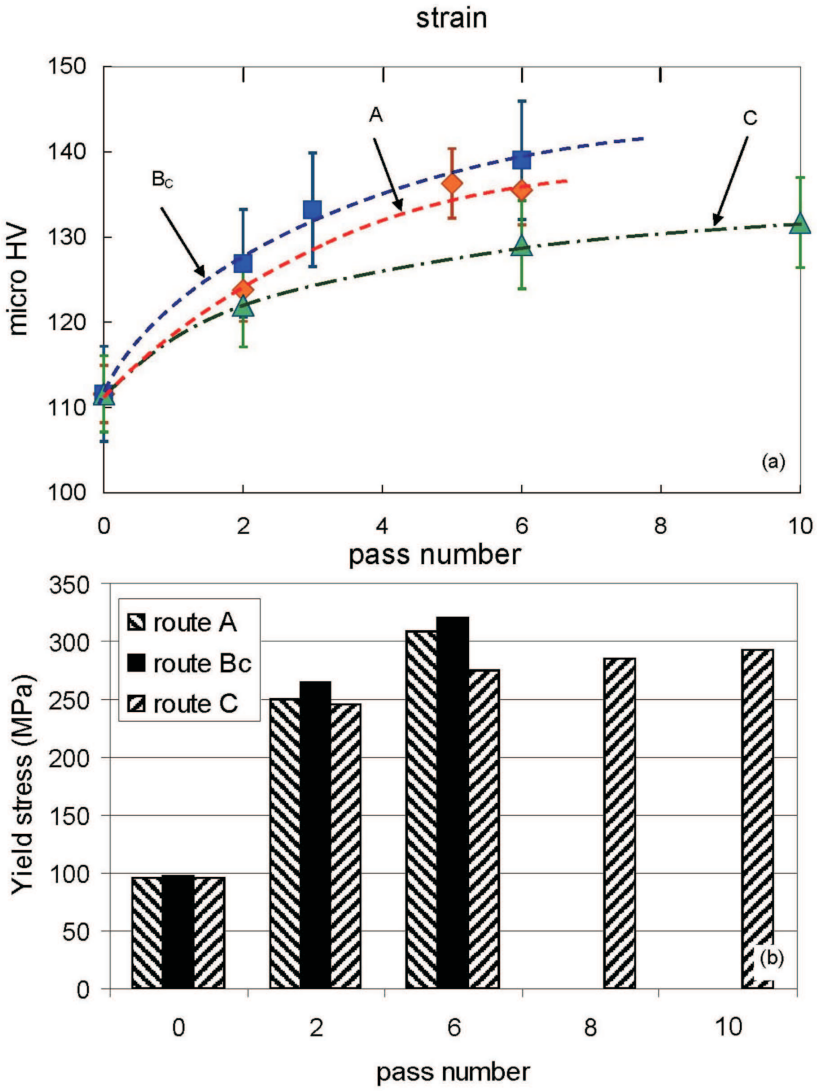

Fig. 3. (a) Plot of microhardness and (b) plot of yield stress as 'functions' of number of passes in ECAP, for different routes

After the orthogonal changes were applied (route B_C), the increase of the internal stresses after the first 3 passes (Fig. 3b) led directly to sample cracking. However, the macro-cracks were also observed in the 'softer' samples deformed through route A after 5 passes, as presented in Fig. 2. In the samples deformed through route C after 10 passes, only micro-voids were observed, mainly close to the large SPP (Fig. 4). The above observations agree well with the detailed work by Lapovok et al [26] on the ECAP-processed titanium. They showed that the generation of the voids started from one pass of deformation, in particular, when routes A and B_C were applied.

3.2. Global texture measurements

The global texture measurements were carried out in the section perpendicular to ED. In the present study, Miller indices {*hk l*}<*uvw*> denote the texture component which has the {*h k l*} plane parallel to the ED-plane (the normal of ED-plane is parallel to ED) and the <*uvw*> direction parallel to ND, characteristic for the last deformation pass.

The {111} pole figures depicting the texture evolution as a 'function' of the applied deformation mode are presented in Fig. 5. The initial material was characterized by very weak texture components. In the case of schemes A5x and B3x (the meaning of the applied notation is as follows: deformation in 5 and 3 passes by routes A and B_C, respectively) the tendency to increase the density of the texture components within a broad scattering of the {110}<112>-type orientation was observed[1)]. Both schemes led to two symmetrical positions of that orientation, although, in the case of route B_C after three passes, one of them was stronger.

For the samples processed through route C, nearly the same two complementary orientations close to {110}<112> (with a well-marked rotation around TD), of equal intensity, were observed within a broad range of deformations. However, as the pass number increased, the maximum intensity of the {111} plane normals decreased (e.g. for the samples processed through route C, from 6.1 to 4.8 and 3.0 after 2, 6 and 10 passes, respectively). Another common effect observed resulted from the significant increase of the density of the {111} plane normals close to TD.

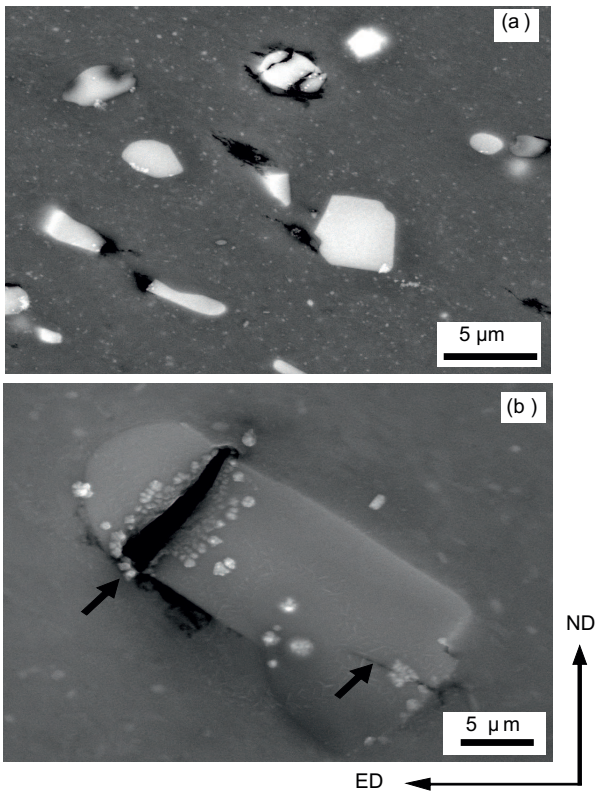

Fig. 4. (a) Micro-cracks inside matrix and close to large SPP, (b) cracks of large particles. Sample deformed through route C after 10 passes. Imaging in back scattered electrons in SEM

[1)] The orientations are defined with respect to the coordinate system characteristic for the section perpendicular to ED, characteristic for the last deformation step, in accordance with the scheme presented in Fig. 1.

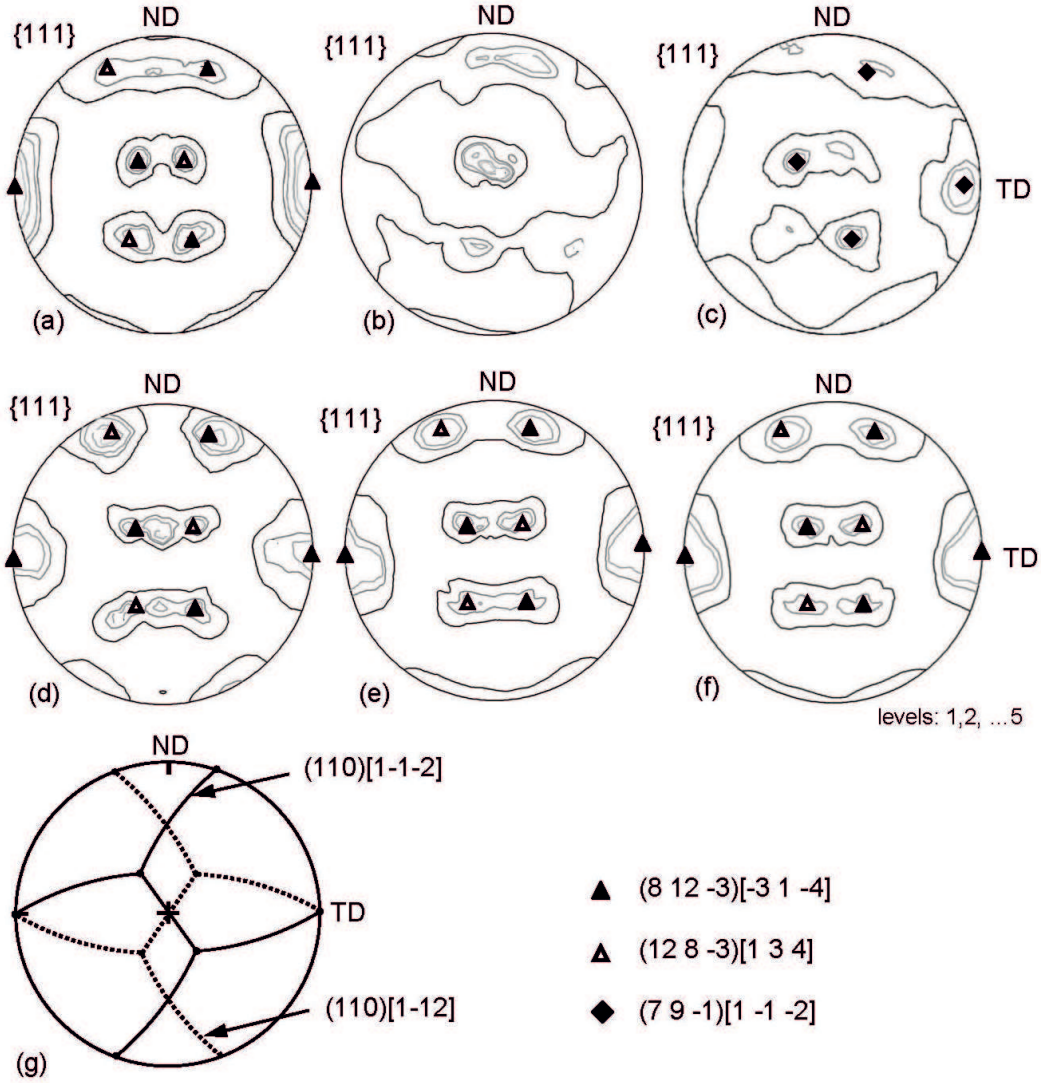

Fig. 5. {111} pole figures showing global texture development in samples processed by schemes: (a) A5x, (b) B2x, (c) B3x, (d) C2x, (e) C6x, (f) C10x. (g) Schematic presentation of two symmetrical components of {110}<111>-type. X-ray diffraction in the plane perpendicular to ED

For routes A and C, the first pass texture is retained in the subsequent passes, apart from the slight variations in the strengths of the main texture components, as observed earlier by Li et al [27, 28] and Beyerlein and Langdon [29] in polycrystalline copper. This leads to the conclusion that, despite the different distortions of the grains, the textures obtained for these routes and within a broad range of strains were generally similar. This also indicated that the deformation of the grains under the shear in ECAP (for A and C routes) did not noticeably affect their rotations, as it was earlier pointed out by Segal [30]. For route B_C, the main texture components varied both in the positions and the intensity, probably due to the complexity of the deformation imposed by the B_C route. This was well-visible when schemes B2x and B3x were compared. However, after three passes, the main texture components were similar to those observed in the samples deformed along schemes A or C.

3.3. TEM analysis of the dislocation structure development

In the ECAP processed AA3104 alloy, two effects of the shear were observed. The first effect was due to the applied deformation scheme, which determined the different configuration of the shear plane, with respect to the pre-existing dislocation barriers, formed in the earlier passes. The second one was related to the presence of the large SPP and the formation of highly deformed zones around the particles. For a detailed space distribution of the highly dislocated areas, i.e. the shear bands and the

deformed zones around large SPPs, the specimens were inspected by TEM over two sections, i.e. one perpendicular to TD and the other – to ED.

3.3.1. The influence of the deformation scheme

Section perpendicular to ED. The microstructures observed in the ND-TD section at a low deformation level showed that the structure refinement had taken place in a significant amount of grains. The initial grain size of 50-60 μm strongly decreased and, after the first two passes, the thickness of a large fraction of the elongated subgrains was below 200 nm.

At low deformation levels, the structures were relatively heterogeneous and very often, a mixture of slightly deformed and highly dislocated areas were observed. After two passes, independently of the applied deformation route, the primary grain boundaries could still be found. This is visible in Fig. 6, showing the microstructures observed in the ND-TD section. After the subsequent passes, the primary boundaries disappeared and the structure appeared to be more homogeneous. The amount of grains in the ultrafine range increased, but the further (> 2 passes) grain refinement was significantly slower.

In the case of route A (after 5 passes, strains of 5) the microstructures were composed of strongly elongated subcells (in fact, nanolayers) of 200-300 nm in thickness, with the boundaries situated nearly parallelly to TD (Fig. 7a). After 3 passes (strains of 3) in the samples deformed by route B_C, a nearly equiaxed microstructure (Fig. 7b) is observed. In the case of the samples processed along route C, the original grains also rapidly subdivided, even at low strain levels, by forming high angle boundaries (Fig. 8a-c). The TEM local orientation measurements along the line scan parallel to ND documented that the misorientation between the neighbouring grains very often reached 50-55°, as visible in Figs. 8d-e. The process coincided with the thickness decrease of the layers of the similar orientation. The structure of the nanolayers broke down to a finer one at very high deformations. However, similarly to the case of routes A and B_C, the subgrain size in ND (or more precisely, the spacing between the lamellas) tended to stabilize after 2-3 passes (strains of 2-3); in the subsequent passes, the amount of grains in the ultrafine range increased slowly. When schemes A5x and C10x are compared, despite of the significant difference in the applied final deformation, no visible differences in the final microstructures were observed. In both cases, the microstructures were composed of fine 200-300 nm thick grains, elongated in TD.

Section perpendicular to TD. The microstructures observed in the longitudinal, that is the ND-ED section showed well-marked shear bands crossing the pre-existing structure of the microbands. For the samples processed through routes A and B_C, after 5 and 3 passes, respectively, the microstructures observed in this section were qualitatively similar[2)]. As an example, Fig. 9a shows the microstructure observed in the sample deformed along route A after 5 passes. The newly created *copper-type* shear bands [31, 32], 1-5μm in width,

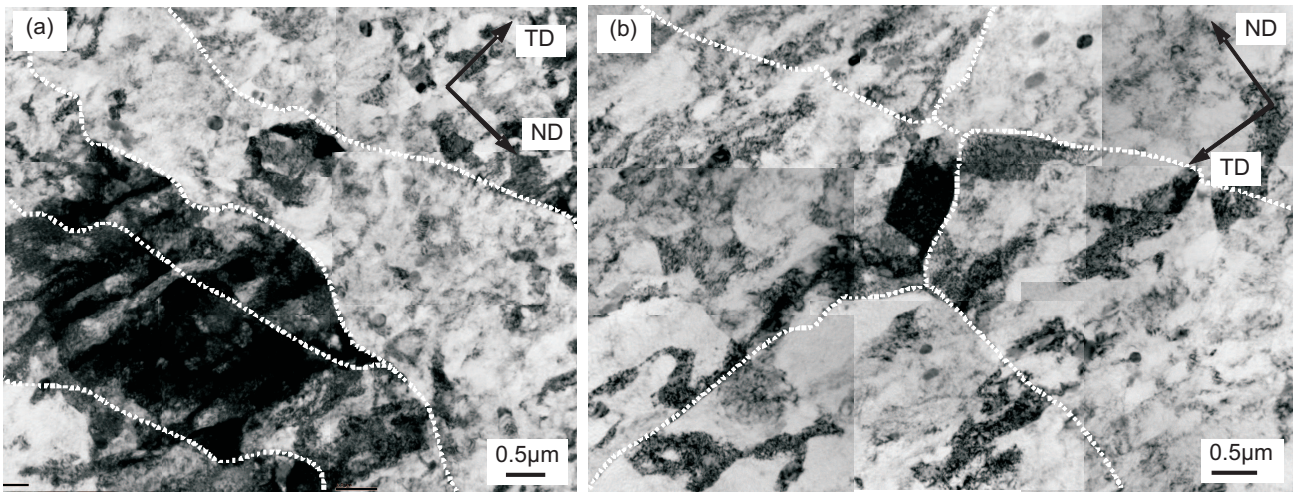

Fig. 6. TEM microstructures observed in ND-TD section showing the presence of primary grain boundaries (dotted lines). Samples deformed along (a) B2x and (b) C2x schemes

[2)] Prangnell et al [15] in the Al-3%Mg alloy, after an orthogonal change in the strain path, following the processing through two extrusion cycles by ECAP, using route B_C, also observed (in the ND-ED section) clusters of shear bands crossing several grains.

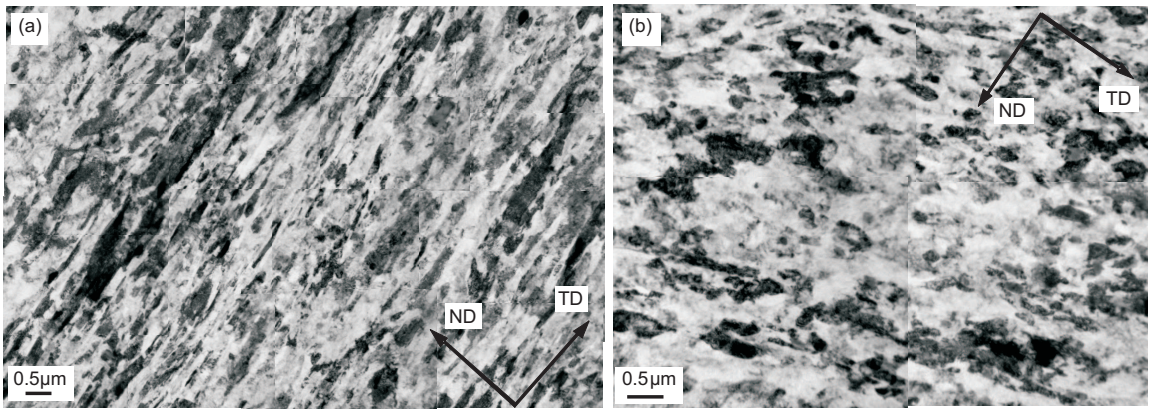

Fig. 7. TEM microstructures observed in ND-TD section showing (a) elongated subgrains in sample processed through scheme A5x and (b) nearly equiaxed structure of sample processed through scheme B3x

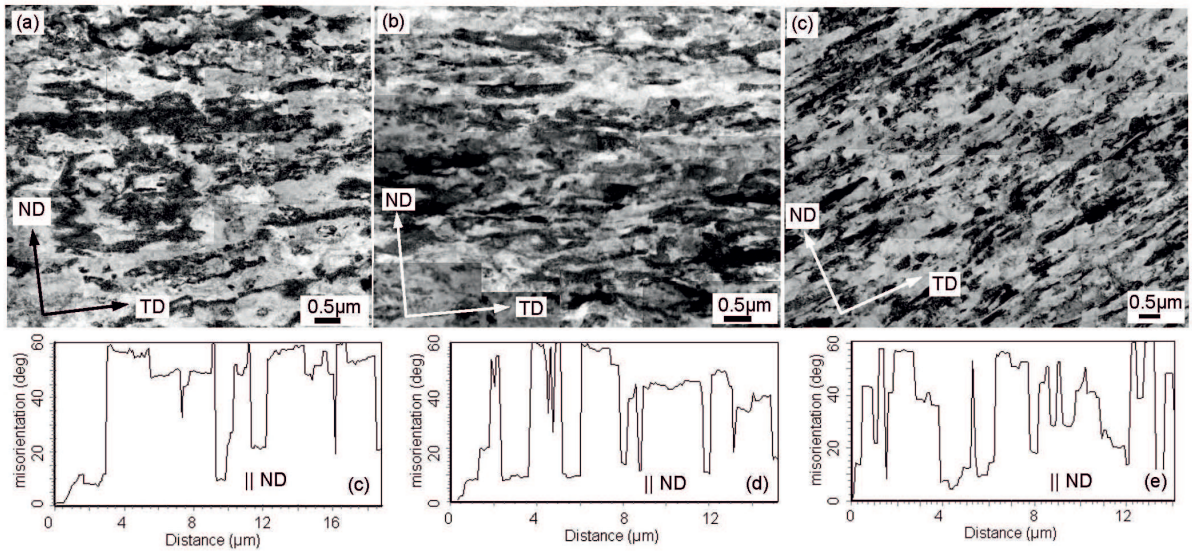

Fig. 8. TEM micrographs showing microstructure development in ND-TD section. Samples deformed along: (a) C2x, (b) C6x and (c) C10x schemes. (d) – (f) Misorientation profiles along ND with respect to the first point. Local orientation measurements in TEM. Step size of 30 nm

cross the pre-existing structure of the microbands or the shear bands formed in the earlier passes. Those elongated structures underwent a further breakup in the successive passes by means of shearing along the planes parallel to TD. As a consequence of the localized shear, a strong curvature of the microbands was observed in the vicinity of the shear bands (Fig. 9b).

The internal microstructure of the shear bands was composed of thin subcells (50-100 nm thick), elongated in the shear direction. The thickness of the background structure of the elongated cells observed in this section was within the range of 100-200 nm. The local microtexture within the shear bands was different from that outside the band (Fig. 9c and d). Consequently, the traces of the {111} planes within and outside the bands were quite different. The traces of the background structure of the elongated cells, observed in Fig. 9a, were inclined by 0-10° to ED. When the shear banding appeared along the line inclined by about 35-40° to ED, the {111} pole figures exhibited a pronounced scattering of the orientations identified within the shear band (Figs. 9c and d), which was generally connected with the increase of the trace inclination of one of the {111}-type planes with respect to ED. Because of the localized shearing, a rigid body rotation of about 25-30° (around the axis close to TD, Fig. 9d) of the material occurred inside the shear bands, together with a relative translation of the dislocation boundaries outside the band (Fig. 9a). The sense of this rotation is such as to incline the increase of the microband plane with respect to ED (this mechanism is analogous to that observed in the twinned structures of the copper-based alloys [33, 34]). It is also well-visible that the orientation scattering as a result of the shear band formation leads to the texture components dominating the global texture.

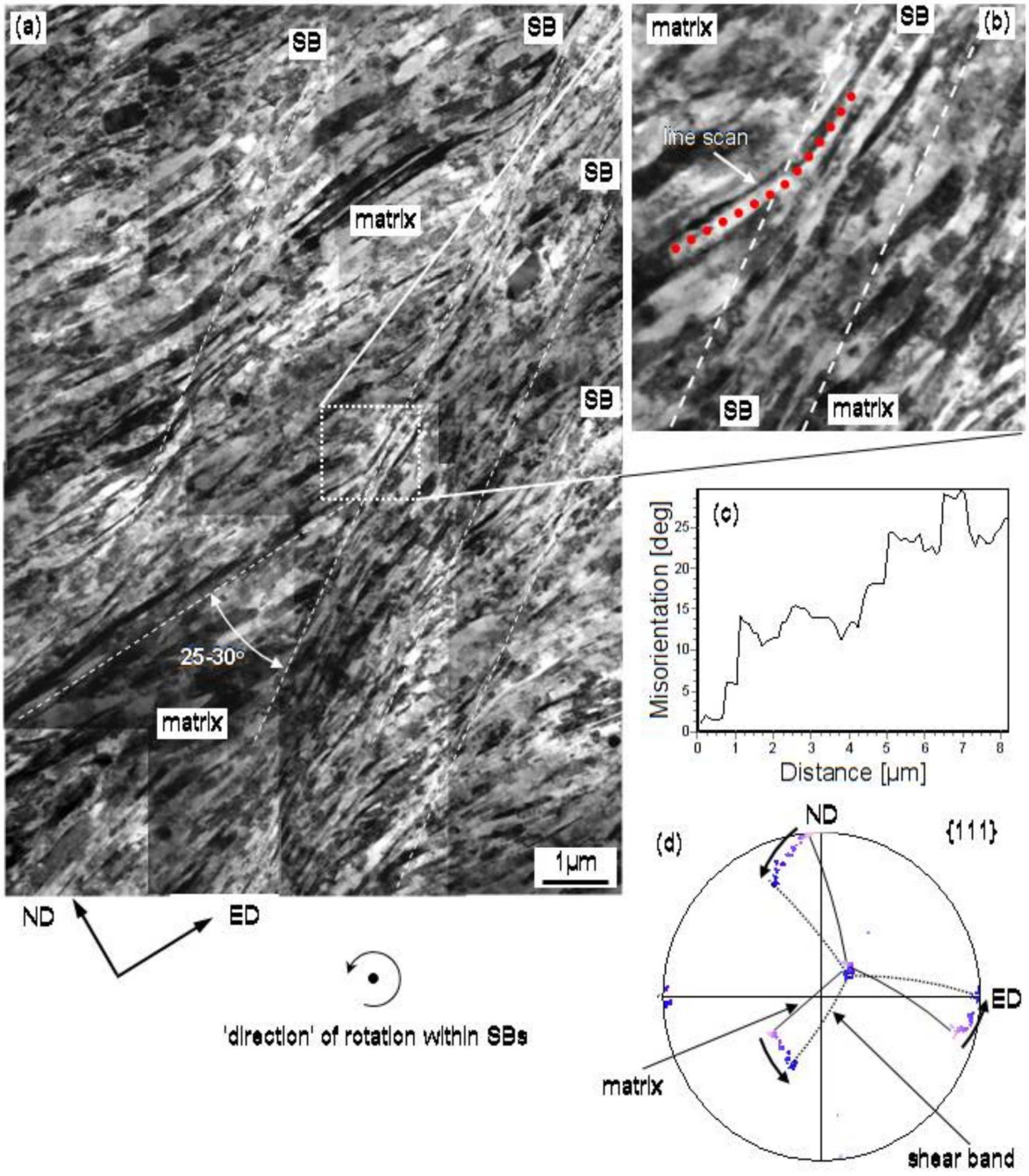

Fig. 9. (a) TEM micrographs showing formation of shear bands in sample deformed through scheme of A5x. (b) Detail from (a) showing incorporation of thin lamella into shear band. (c) The misorientation profile for 'line scan' marked in (b). (d) {111} pole figure showing orientations identified along the line scan within SB and the neighbouring matrix. Local orientation measurements in TEM. ND-ED sample section

Figure 10 shows the microstructure evolution of the sample deformed through route C after 2, 6 and 10 passes observed in the ND-ED plane. A general observation is that the structure refinement was not as intensive as in the case of route A and B_C. At low deformations (after 2 passes) should be corrected the microstructure still depended on the grain orientation and was composed of broad clusters of elongated cells crossed by 'diffuse' shear bands. The thickness of the particular elongated subcells was close to 1μm, whereas the shear bands – a few tens of microns. At higher deformations (as observed after 6 and 10 passes), the microstructure systematically appeared to be more uniform and finer. The 'old' shear bands made traces nearly parallel to ED, whereas the 'newly-formed' ones were inclined by 35-40° to ED.

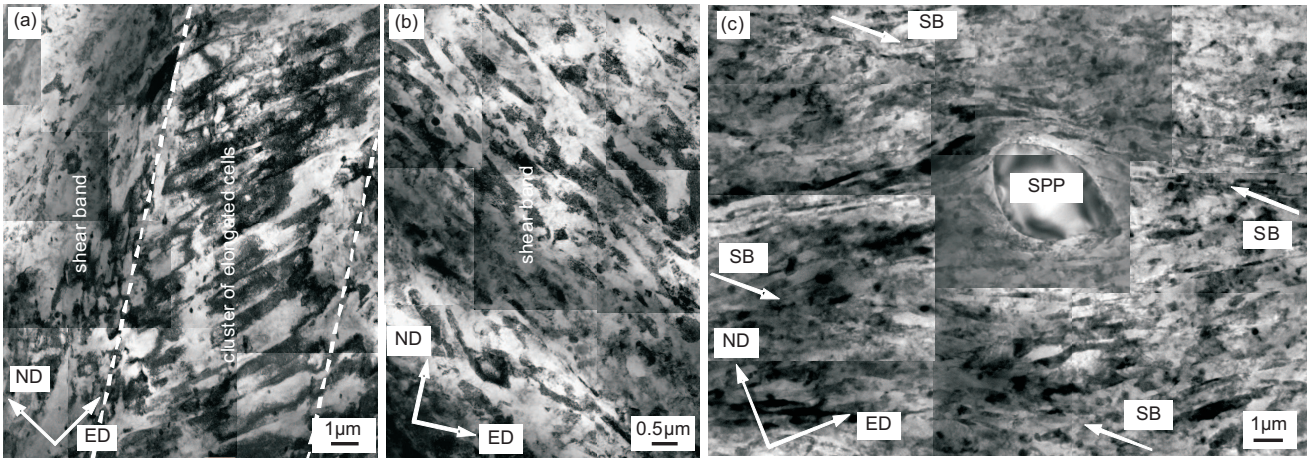

Fig. 10. The development of the microstructure observed in ND-ED section. Samples deformed along: (a) C2x, (b) C6x and (c) C10x schemes. TEM bright field micrographs

3.3.2. The effect of the particles on the deformation microstructure

The AA3104 alloy, in the annealed state, was characterized by a bimodal structure of second phase particles (SPP), i.e. coarse plate-like intermetallics (large SPP) and fine, mostly globular dispersoids. The matrix volumes (solid solution) showed increased contents of Mg, Mn and Cu, whereas both types of particles revealed a significantly more complex chemical composition, due to the strongly increased contents of Mn, Fe, Si with a small addition (in some cases) of Cu and Mg. The diameter of most of the fine dispersoids was in the range of 50-200 nm. The energy dispersive X-ray microanalysis in TEM and SEM showed that the dispersoids were of the AlMnSi, AlMnCu or $CuAl_2$ type. The plate-like intermetallics, in most of the observed cases, were of the AlFeMnSi (very large size) or Al_6Mn type and had sizes in the range of 2-15 μm.

Fine dispersoids (randomly distributed) had a little visible effect on the deformation microstructure evolution of the ECAP-processed samples, independently of the applied deformation route. The observed traces of the cell boundaries at low strains, and the microbands or the shear bands at high strains, were not disturbed by fine dispersoids. However, they could have an effect on the increase of the dislocation density and thus the decrease of the distance between the dislocation boundaries and the increasing misorientation angle between the neighbouring subgrains.

The effect of the large SPP on the deformation microstructure was more clearly visible. Figure 11 shows the TEM bright field images of the areas containing large, almost round or ellipsoidal, SPP in two sections, i.e. ND-TD and ND-ED. At low strain levels, the deformed matrix around the large SPP was only slightly disturbed and relatively homogeneous, except for a very thin layer (<100 nm) in the nearest vicinity of the particles. At larger deformation levels, the strongly disturbed zones around the large SPP became gradually broader. In the case of route A and B_C, the broadening of the deformed zones around the particles was more intensive with respect to route C, as the number of passes increased. As observed in both sections, the thickness of the strongly disturbed and refined zone was 0.5-2 μm (after 10 passes). The broadening of the deformed zone often coincided with cracking or even a fragmentation of the large, elongated particles.

3.4. SEMFEG/EBSD analysis of the as-deformed state

The complementary analysis of the structure and the texture development was performed in the ND-TD section, by a high resolution SEM equipped with the EBSD facility. The results of the orientation mapping of the samples deformed through routes A or B_C were completely unsatisfactory. A high level of internal stresses led to blurred Kikuchi patterns and to very poor orientation maps. Only in the case of the samples processed through route C, the orientation maps contained a satisfactory quantity of correctly indexed points. For relatively low deformations (up to 2 passes), the diffraction pattern quality was sufficient to resolve about 90% of the diffraction patterns. After higher strains, the quality decreased so that for the samples deformed to strains ~10 (10 passes), this ratio was ~75-80%.

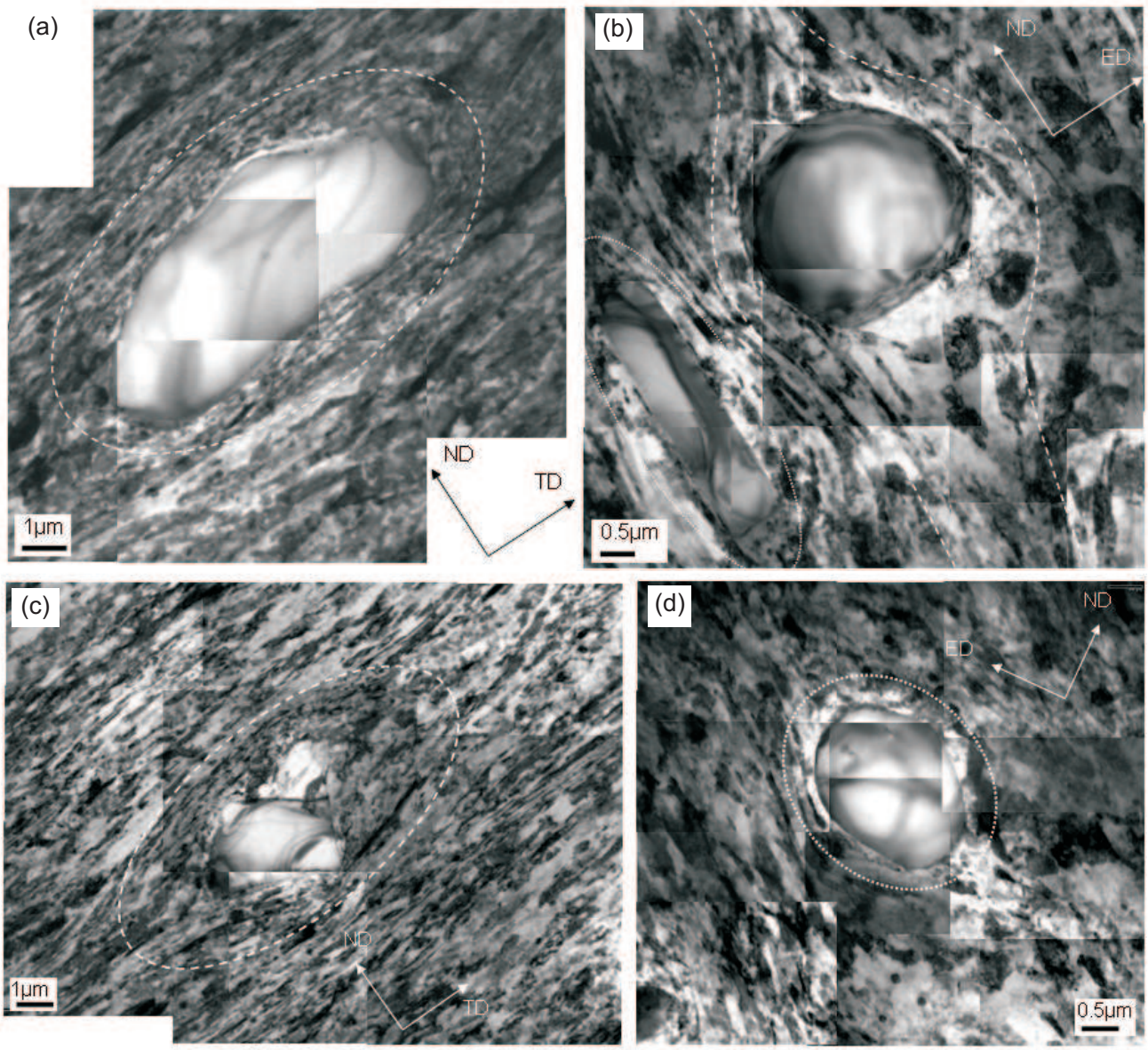

Fig. 11. Typically observed microstructures around large SPP; (a) and (b) samples deformed along scheme of A5x, (c) and (d) sample deformed along scheme of C6x. TEM bright field images showing microstructures observed in: (a) and (c) ND-TD section, (b) and (d) ND-ED section

Figures 12a-c show the high resolution EBSD maps measured for the samples after 2, 6 and 10 passes. (These 100μm×100μm images were created with the step size of 100 nm). In the ND-TD section, the microstructure consisted of grains elongated in TD. Even at low deformations ($\leqslant$2 passes), the boundaries between the cell blocks, inside the primary grains, had segments that already exceeded 15° in misorientation[3)].

The average boundary spacing in ND systematically decreased as the deformation increased; it was about 0.5-2 μm and 0.2-0.4 μm after 2 and 10 passes, respectively. However, the high angle spacing in TD was considerably larger and could be estimated to be within the range of 10-20 μm and 1-5 μm after 2 and 10 passes, respectively. In most of the observed cases (in ND-TD section), the average aspect ratio was within the range of L_{TD}/L_{ND} =~2-10 and L_{TD}/L_{ND} = 5-12.5 for the samples deformed in 2 and 10 passes, respectively.

The {111} pole figures corresponding to the orientation maps, shown in Figs. 12d-f, are presented in the same ND-TD coordinate system. The tendency to form the texture components within a broad scattering of the {110}<112> orientation was evident, as previously identified in the X-ray measurements. (Additionally, other

[3)] High angle boundaries are defined as having the misorientations greater than or equal to 15°, whereas low angle boundaries are defined as having the misorientations of less than 15°.

minor components were observed). At higher deformations, two nearly symmetrical positions of that orientation were clearly visible (usually, slightly deviated from the ideal positions (of {110}<112>) by the TD or/and ND rotation). The orientation maps showed traces of thin layers of alternative orientations. A significant part of those planar dislocation arrangements was aligned along the ED-TD planes and coincided with the crystallographic {111}-type planes.

The average grain diameter calculated for the samples deformed by route C after 2, 6 or 10 passes was estimated to be 5 μm, ~1 μm and 0.7 μm, as is visible in Fig. 13[4]. Evidently, the maximum of the grain size (diameter) distributions decreased as the applied number of passes increased. It is evident that those calculations were not 'sensitive' to the shape of grains and were affected by the 'quality' of the orientation maps. The quantity of unresolved (or incorrectly indexed) points in the samples after 10 passes (~20%) is higher than after 2 passes (~10%). However, the random distribution of incorrectly indexed points does not constitute a limitation factor; a significant part of these so-called 'spikes' is removed from the orientation maps after the standard procedure (implemented into the TSL software) of 'cleaning'.

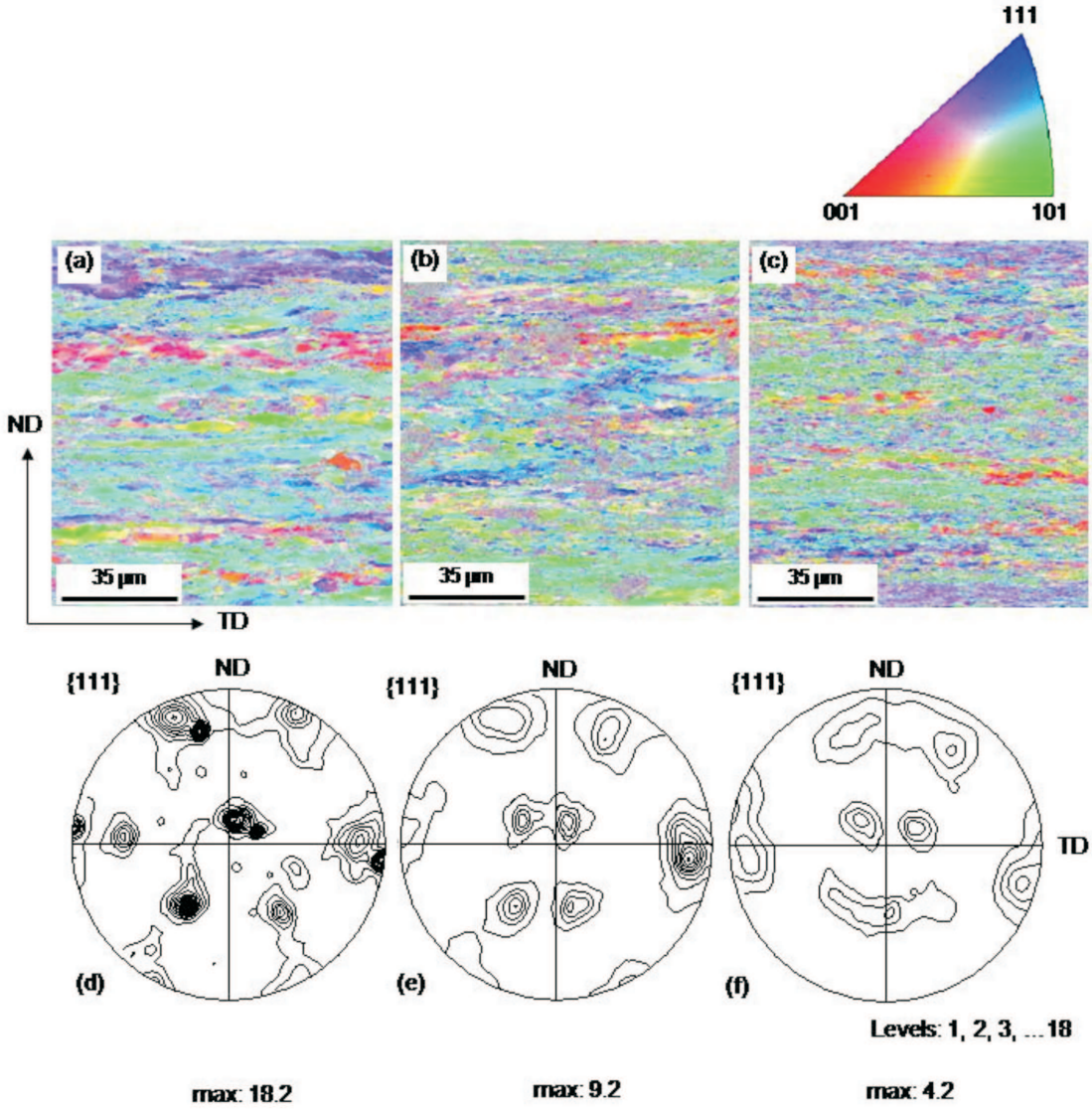

Fig. 12. SEMFEG/EBSD mapping of the samples deformed through route C after: (a) 2, (b) 6 and (c) 10 passes, and (d) – (f) corresponding {111} pole figures. Local orientation measurements in the plane perpendicular to ED. Inverse pole figure colour code is applied. Step size of 100 nm

[4] In these calculations the critical misorientation between the pixels was 2°.

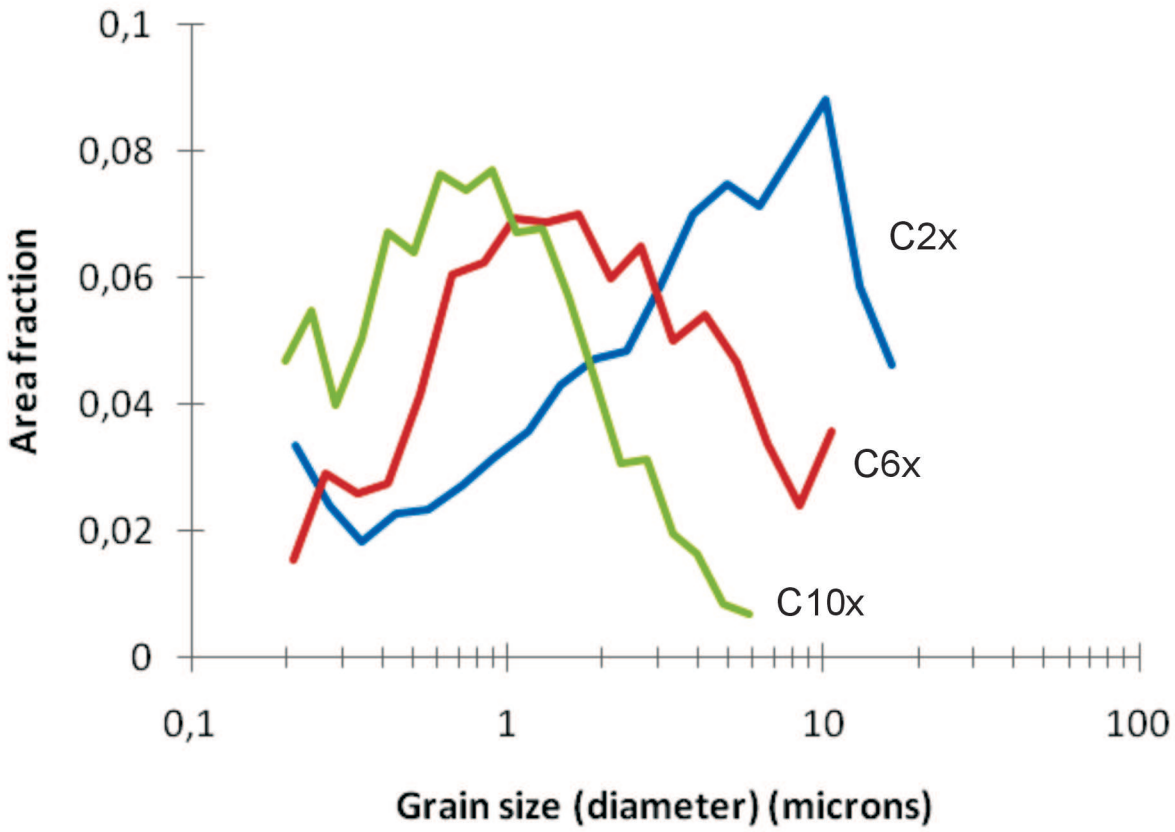

Fig. 13. The distribution of grain size for samples processed through route C. Local orientation measurements by SEMFEG/EBSD in the plane perpendicular to ED. Step size of 100 nm

4. Discussion

4.1. Shear banding in the ECAP processed samples and textural changes

In the past, crystal subdivision was extensively reported but mostly by the studies on only one section, using either TEM or SEM-EBSD; only limited works were delivered, eg. [2, 10] on the structure characterization over two or three sections. In the present contribution, in order to provide a better description of the space distribution of the dislocation boundaries, a systematic study of the deformation microstructure of two perpendicular surfaces was carried out. Due to the early decomposition of the samples processed by routes A and B_C, a direct comparison of the microstructures was possible only for the first three passes. It was well-documented that routes A and C did not readily lead to the creation of a material that could be described as having an equiaxed structure; the TEM images taken of two perpendicular sections clearly indicated the formation of planar dislocation arrangements resembling flat grains. The distribution of the grains was fairly equiaxed (in the ND-ED section) only in the sample processed via route B_C. This route led to a more broken-up microstructure, as previously observed, e.g. by Mishra on copper [10] or Furukawa et al [2] on pure aluminium.

In a macroscopic scale, all the deformation routes led to macroscopic inhomogeneities of the plastic flow. The so-called '*copper-type*' shear bands [31, 32] were formed against the background of the planar dislocation structures (flat grains) as the precursory obstacles. The formation of the successive generation of shear bands crossing the earlier formed dislocation arrangements directly led to the microstructure refinement. The observations of the microstructure changes provided a basis for a discussion on the origin and nature of the micro- and macro- scale strain localizations and their influence on the structure refinement.

In the analysed alloy, the shear bands in slightly deformed structures (after 1^{st} pass) were not observed, independently of the applied deformation scheme. That led to the conclusion that the contribution of the substructure of the dislocation cells with their relatively isotropic properties was not justified in the shear bands formation. The microscopic observations of many channel-die compressed metals indicated that the shear banding was preceded by a formation of obstacles for a homogeneous dislocation glide in the particular crystallites [31-34]. As the deformation continued and the misorientation

increased, those primary cells became flat subgrains[5]. Step-by-step, the boundaries became sharper due to the higher dislocation density and they gained a grain boundary character. They acted also as barriers for the dislocation motion and became gradually less penetrable by the dislocations operating in the planes crossing the highly dislocated planar structures (Fig. 14a).

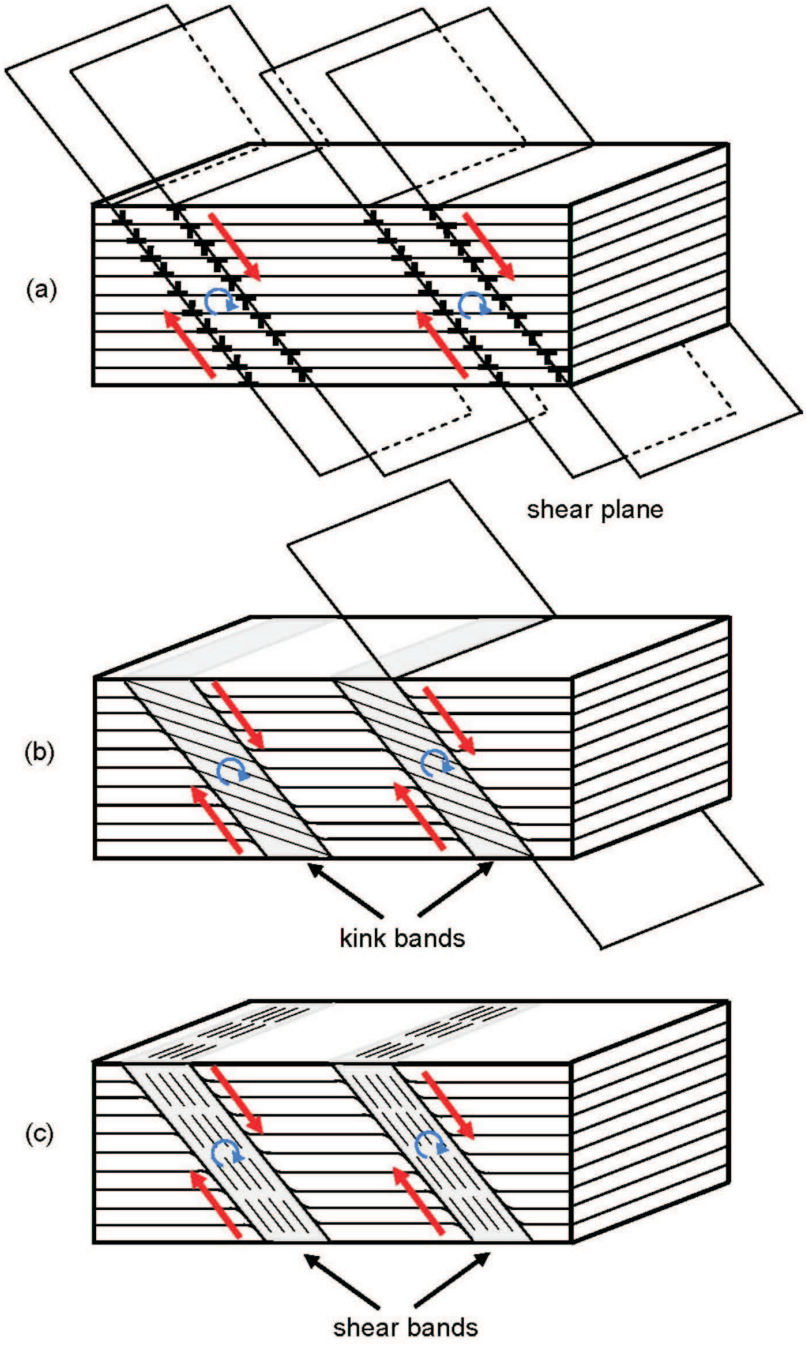

Fig. 14. Schematic presentation of shear band formation in ECAP-processed samples through routes A and C. (a) The increase of the dislocation density of alternate sign at the border of potential shear band leading to (b) formation of kink-type bands. (c) Localized shear along shear band plane in re-oriented areas of shear band. Shear stresses lead to strictly defined re-orientation of matrix within the shear band area

[5] This is deduced from the observations on both analyzed sections.

It was a crucial moment for the occurrence of shear bands. Paul et al [31-34] stated that the formation of the anisotropic planar dislocation structures of nanolayers (twin/matrix or elongated subcells) was the necessary condition for the shear banding in the fcc metals. Those planar structures were seen in many metals subjected to high strains, as reported e.g. by Gil Sevillano et al. [33], Bay et al. [36], Hughes and Hansen [37]. It is also well-known that the larger the deformation, the stronger the anisotropic properties of the dislocation structures, e.g. [37-40], and the more increased the tendency to strain localization [38]. Those strong anisotropic properties were especially gained by the material after the change of the deformation path, leading very quickly to shear banding, as presented recently by Paul et al [41], in the plane strain compressed single copper crystals of the initial Goss{110}<001> orientation.

The crystal lattice rotation within the shear band (and the kink-band formation), as observed in Fig. 14b (and Fig. 9b), explains why the shear band plane is quite different from the {111} planes in the matrix outside the band. The highly dislocated boundaries (the boundaries of elongated subcells or the earlier formed shear bands) are thought to be an effective barrier for the dislocation motion on the slip planes which cross the boundaries. This consequently, causes a high stress concentration at the boundaries up to the point when the dislocations break through the pre-existing structure and create a localized slip in the form of a shear band (Fig. 14c). The strictly defined crystal lattice rotation within the shear band area (Fig. 14b) increases the inclination of the microband planes with respect to ED. The observed kink bands are precursor to the shear band formation. As a result of a localized deflection, the orientation of the crystal lattice is observed to change progressively, as observed in Fig. 9b–d. This brings the imposed plastic deformation to be accommodated through an inhomogeneous mechanism of shear banding, according to the mechanism proposed in [33, 34]. The supposition that the planar dislocation structures are the necessary precursor to the shear band formation in the face centered cubic metals, as suggested many times in the past, e.g. [22-24, 30, 32, 35] on rolled or channel-die compressed metals, is thus strongly supported. When the orthogonal changes in the strain path are used (route B_C), the grain refinement is also strongly influenced by the shear banding[6)]. The repeated introduction of shear bands in two orthogonal planes would explain the formation of very heterogeneous structures observed by Prangnell et al [15] in the Al-Mg alloys and Skrotzki et al [16] in pure Al. However, from the point of view of the final properties, more important is how the annealing can lead from the planar dislocation structures produced by ECAP to the ultra fine and equiaxed grain structure [42].

4.2. The influence of the second phase particles

In the two-phase alloys, the SPP were another factor which induced large lattice rotations. At low deformations, the microstructure evolution strongly correlated with the grain orientation, whereas at large deformations, significant orientation gradients occurred in the nearest neighborhood of the particles. The width of the deformed zones close to the large SPP strongly depended on the size of the particles; the larger the size, the larger the thickness of the strongly disturbed zone.

The AA3104 alloy contains a bimodal structure of SPP. Fine dispersoids have a little visible effect on the dislocation arrangements, especially at low deformations. The dislocation structure development of the dispersoids containing alloys differs from that observed in the single-phase material. These differences are mainly due to the weaker and more diffuse boundaries that prevent the formation of the planar dislocation arrangements in the particle containing an alloy. Apps et al [20] on model Al-0.2%Sc and Al-0.13%Mg alloys showed that the presence of a high density of non-shearable small particles delays the formation of the cell band structure and decreases the tendency to strain localization. This, in turn, delays the formation of a uniform submicron grained microstructure by shear banding. In the case of the fine dispersoids, the most important parameter which influenced the deformation behaviour is the interparticle spacing or, more precisely, its relation to the diameter of the dislocation cell [23, 43]. However, when the influence of the dispersoids and the large SPP is compared separately, the structure refinement is more readily found in the volumes with small particles than in the material with larger ones, as showed earlier by Dai et al. [19] on the ECAP-processed AA2024 aluminium alloy.

Other problems are related to the void nucleation in the highly deformed materials. The grain refinement and the increase in the density of the triple junctions due to the formation of ultrafine grains lead to the increase of the availability of void nucleation sites, as reported by Lapovok et al [26], on titanium. The volume fraction of the voids in pure metals decreases when the backpressure is applied. In the particle-reinforced alloys and in the case when the backpressures do not play any important role (as in the present case), intensive nucleation of the voids is expected not only at the triple point junctions but also at the particle/matrix interfaces

[6)] The microstructures observed in the ND-ED sections for routes A and B_C are similar

(Fig. 4a). Stolyarov and Lapovok [44], in the AA5083 alloy processed through route $B_{C,}$ showed that in the absence of backpressure or when its value is low, the samples had cracked after the first ECAP pass and had failed during the second pass.

5. Conclusions

The deformed microstructure and the microtexture developed during the ECAP processed AA3104 alloy has been investigated with the use of TEM and SEM-FEG. The following conclusions can be drawn:

- The TEM observations and the SEM/EBSD local orientation measurements showed that all three deformation routes led to a strong structure refinement. In the ND-TD section, only in the case of route B_C nearly equiaxed grains were observed just after three passes. In the ND-ED section, the subgrains were still strongly elongated, even in route B_C. In the case of routes A and C, a misoriented planar dislocation structure of nanolayers was spotted. The misorientations created between the neighbouring flat subgrains very often reached 40-55°.
- These elongated dislocation structures undergo further breakup in the successive passes by shearing along the planes parallel to TD. The kink-type bands are considered to be the precursors of the shear bands leading to strong crystal lattice rotations. As the strain becomes localised, a rotation takes place in the bands and the background structure of the flat grains rotates away from the ED-TD plane. The crystallographic relation between the matrix outside the band and the interior of the freshly formed shear bands is associated with the rotation of the crystal lattice around the axis close to TD.
- It was demonstrated that irrespective of the applied deformation routes, large, not deformable, second phase particles strongly influenced the strengthening of the matrix. The structural inhomogeneities in the form of deformation zones occurring near the coarse particles led to significant local distortions of the deformed microstructures. The fine dispersoids had a little visible effect on the dislocation arrangements, especially at low deformation levels.
- The texture evolution was found to follow nearly the same 'course' for different routes of ECAP, apart from the slight variations in the strengths and the exact position of the main texture components. All the deformation routes led to the strong density of the <112> and <110> poles close to ND and ED, respectively.

Acknowledgements

The authors acknowledge the financial support from the Ministry of Science and Higher Education (Grant no. R15 048 03) and are grateful to Dr A. Tarasek for his help in the ECAP, Dr W. Wajda for the help in the mechanical tests and Miss M. Miszczyk for the thin foil preparation.

REFERENCES

[1] R.Z. Valiev, R.K. Ismagiliev, I.V. Alexandrov, Prog. Mat. Sci. **45**, 103 (2000).
[2] M. Furukawa, Z. Horita, M. Nemoto, T.G. Langdon, Journal of Materials Science **36**, 2835 (2001).
[3] R.Z. Valiev, T.G. Langdon, Prog. Mat. Sci., **51**, 881 (2006).
[4] Y. Iwahashi, Z, Horita, M. Nemoto, T.G. Langdon, Acta Mater. **45**, 4733 (1997).
[5] A. Gholinia, P.B. Prangnel, M.V. Markushev, Acta mater. **48**, 1115 (2000).
[6] W.J. Kim, J.K. Kim, T.Y. Park, S.I. Hong, D.I. Kim, Y.S. Kim, J.D. Lee, Metall. Mater, Trans. **33A**, 3155 (2002).
[7] F.D. Tore, R. Lapovok, J. Sandlin, P.F. Thompson, C.H.J. Davis, E.V. Pereloma, Acta Mater. **52**, 4819 (2004).
[8] B. Cherukuri, T.S. Nedkova, R.A. Srinivasan, Mat. Sci. Engn. **410-411**, 394 (2005).
[9] H. Paul, T. Baudin, A. Tarasek, M. Miszczyk, Solid State Phenomena **160**, 265 (2010).
[10] A. Mishra, V. Richard, F. Gregori, R.J. Asaro, M.A. Meyers, Mater. Sci. Engn. A **410**, 290 (2005).
[11] I. Gutierez-Urrita, M.A. Munoz-Morris, I. Puertas, C. Luis, D.G. Morris, Mat. Sci. Engn. **A475**, 268 (2008).
[12] J. Gubicza, N.Q. Chin, J.L. Labar, Z. Hegedus, T.G. Langdon, Mat. Sci. Engn. **A527**, 752 (2010).
[13] J. Kuśnierz, M-H. Mathon, T. Baudin, Z. Jasieński, R. Penelle, Mat. Sci. Forum., 851 (2005).
[14] S. Suwas, G. Gottstein, R. Kumar, Mat. Sci. Engn. **A471**, 1 (2007).
[15] P.B. Prangnel, J.R. Bowen, P.J. Apps, Mater. Sci. Engn. **A375-377**, 178 (2004).
[16] W. Skrotzki, N. Sheerbaum, C.-G. Oertel, H.-G. Brokmeier, S. Suwas, L.S. Tóth, Acta Materialia **55**, 2211 (2007).
[17] G.H. Zahid, Y. Huang, P.B. Prangnell, Acta Mater. **57**, 3509 (2009).
[18] M. Reichanian, R. Ebrahimi, N. Tsuji, M.M. Moshksar, Mat. Sci. Engn. **A473**, 189 (2008).
[19] L.H. Dai, L.F. Liu, Y.L. Bai, Materials Letters **58**, 1773 (2004).

[20] B. Hwang, S. Lee, Y.C. Kim, N.J. Kim, D.H. Shin, Mat. Sci. Engn. **A441**, 308 (2006).
[21] P.J. Apps, M. Berta, P.B. Prangnell, Acta Materialia **53**, 499 (2005).
[22] Z. Yao, G. Huang, A. Godfrey, W. Liu, Metall. Mater. Trans. A **40A**, 1487 (2009).
[23] Q. Liu, Z. Yao, W. Liu, Journal of Alloys and Compounds **482**, 264 (2009).
[24] L. Tarkowski, L. Laskosz, J. Bonarski, Mat. Sci. Forum **443-444**, 137 (2004).
[25] J.T. Bonarski, M. Wróbel, K. Pawlik, Materials Science and Technology **16**, 657 (2000).
[26] R. Lapovok, D. Tomus, J. Mang, Y. Estrin, T.C. Lowe, Acta Mater. **57**, 2909 (2009).
[27] S. Li, I.J. Beyerlein, D.J. Alexander, S.C. Vogel, Acta Materialia **53**, 2111 (2005).
[28] I.J. Beyerlein, L.S. Tóth, Prog. Mat. Sci. **54**, 427 (2009).
[29] S. Li, I.J. Beyerlein, D.J. Alexander, Mat. Sci. and Engn. **A 431**, 339 (2006).
[30] V.M. Segal, Mater. Sci. Engn. **A338**, 331 (2002).
[31] P. Wagner, O. Engler, K. Lücke, Acta Metall. Mater. **43**, 3799 (1995).
[32] H. Paul, A. Morawiec, E. Bouzy, J.J. Fundenberger, A. Piątkowski, Microchimica Acta **155**, 243 (2006).
[33] H. Paul, J. Driver, C. Maurice, A. Piątkowski, Acta Mater. **55**, 833 (2007).
[34] H. Paul, A. Morawiec, J. Driver, E. Bouzy, Int. Journal of Plasticity **25**, 1588 (2009).
[35] J.G. Sevillano, P. Van Houtte, E. Aernoudt, Prog. Mater. Sci. **25**, 69 (1981).
[36] B. Bay, N. Hansen, D.A. Hughes, D. Kuhlmann-Wilsdorf, Acta Metall. Mater. **40**, 2005 (1992).
[37] D.A. Hughes, N. Hansen, Acta Mater. **45**, 3871 (1997).
[38] A. Korbel, P. Martin, Acta Mater. **34**, 1905 (1986).
[39] U.R. Andrade, M.A. Meyers, K.S. Vecchio, A.H. Chokshi, Acta Metall. Mater. **42**, 3183 (1994).
[40] M.A. Meyers, G. Subhash, B.K. Kad, L. Prasad, Mech Mater. **17**, 175 (1994).
[41] H. Paul, C. Maurice, J. Driver, Acta Mater. **58**,2799 (2010).
[42] J.R. Hayes, P.B. Prangnell, P. Bate, in: Y.T. Zhu, T.G. Langdon, R.S. Mishra, S.I. Semiatin, M.J. Saran, T.C. Lowe eds.), Ultrafine Grained Materials II, TMS, 495 (2001).
[43] F.J. Humphreys, M. Hatherly, Recrystallization and Related Phenomena, second ed., Pergamon Press, Oxford, 2004.
[44] V.V. Stolyarov, R. Lapovok, Journal of Alloys and Compounds **378**, 233 (2004).

Received: 10 December 2010.